Positronium signature in organic liquid scintillators for neutrino experiments

D. Franco,[1,*] G. Consolati,[2] and D. Trezzi[3]

[1]*Astroparticule et Cosmologie APC, 10 rue Alice Domon et Leonie Duquet, F-75205 Cedex 13, Paris, France*

[2]*Dipartimento di Fisica, Politecnico di Milano, Piazzale Leonardo da Vinci 32, I-20133 Milano, Italy*

[3]*Dipartimento di Fisica, Università and INFN Milano, via Celoria 16, I-20133 Milano, Italy*

(Received 27 November 2010; published 27 January 2011)

Electron antineutrinos are commonly detected in liquid scintillator experiments via inverse β decay by looking at the coincidence between the reaction products: neutrons and positrons. Prior to positron annihilation, an electron-positron pair may form an orthopositronium (o-Ps) state, with a mean lifetime of a few nanoseconds. Even if the o-Ps decay is speeded up by *spin-flip* or *pick-off* effects, it may introduce distortions in the photon emission time distribution, crucial for position reconstruction and pulse shape discrimination algorithms in antineutrino experiments. Reversing the problem, the o-Ps-induced time distortion represents a new signature for tagging antineutrinos in liquid scintillator. In this article, we report the results of measurements of the o-Ps formation probability and lifetime for the most used solvents for organic liquid scintillators in neutrino physics (pseudocumene, linear alkyl benzene, phenylxylylethane, and dodecane). We characterize also a mixture of pseudocumene +1.5 g/l of 2,5-diphenyloxazole, a fluor acting as wavelength shifter. In the second part of the article, we demonstrate that the o-Ps-induced distortion of the scintillation photon emission time distributions represent an optimal signature for tagging positrons on an event by event basis, potentially enhancing the antineutrino detection.

DOI: 10.1103/PhysRevC.83.015504 PACS number(s): 14.60.Pq, 13.15.+g, 34.80.Lx, 29.40.Mc

I. INTRODUCTION

Electron antineutrinos are produced in β decays of naturally occurring radioactive isotopes in the earth, representing a unique direct probe of our planet's interior. Recent results by Borexino [1] and KamLAND [2] have been combined to provide the first observation of geoneutrinos at 5 σ [3]. Also nuclear reactors provide intense sources of antineutrinos, which come from the decay of neutron-rich fragments produced by heavy element fissions. In the past, reactor antineutrinos allowed the neutrino oscillation parameters in the solar sector to be constrained [4]. Presently, several experiments (Double Chooz [5], Daya Bay [6], RENO [7]) exploit reactor antineutrinos to investigate the last unknown neutrino oscillation parameter, Θ_{13}. Moreover, reactor antineutrinos are directly linked to the fissile isotope production and consumption processes and can be studied for monitoring the nuclear plants [8].

One of the main advantages in detecting electron antineutrinos is the clean signature provided by the inverse β-decay reaction

$$\bar{\nu}_e + p \rightarrow n + e^+ \tag{1}$$

by looking at the neutron-positron coincidence.

In organic liquid scintillators, neutrons are captured mainly on protons and identified by looking at the characteristic 2.223-MeV γ ray emitted in the reaction

$$n + p \rightarrow d + \gamma. \tag{2}$$

To enhance the neutron detection, scintillators can be loaded with high neutron capture cross-section materials, like gadolinium. The neutron mean capture time varies from a few tenths up to hundreds of microseconds.

Positrons interacting in liquid scintillator may either directly be annihilated with electrons or form positronium (Ps) [9], a bound state of a positron and an electron with two substates: 25% of positronium populates the spin singlet state ($S = 0$), called parapositronium (p-Ps), and 75% of positronium populates the spin triplet state ($S = 1$), called orthopositronium (o-Ps). p-Ps annihilates by emitting two γ rays of 511 keV with a mean lifetime of 125 ps in vacuum. o-Ps emits three γ rays, with a total energy equal to twice the electron mass and a mean lifetime in vacuum equal to $\sim$140 ns.

In matter, however, interactions of o-Ps with the surrounding medium strongly reduce its lifetime: processes like chemical reactions, *spin-flip* (ortho-para conversion at paramagnetic centers), or pick-off annihilation on collision with an antiparallel spin electron lead to the two-body decay with lifetimes of a few nanoseconds. The surviving three-body decay channel is typically reduced to a negligible fraction.

If the delay introduced by the positron annihilation lifetime is of the order of a few nanoseconds, calorimetric scintillation detectors, like Borexino [10] and KamLAND [11], are unable to disentangle the energy deposited by positron interactions from that released by annihilation γ rays. In these cases, a delayed γ-ray emission induces a distortion in the time distribution of detected photoelectrons (*pulse shape*), with respect to a direct annihilation event. Such a distortion can affect algorithms based on the pulse shape, like position reconstruction and particle discrimination.

Distortions in positron pulse shapes affect not only antineutrino detection via inverse β decay, but also the reconstruction of β^+-decay events, like those from cosmogenic ^{10}C and ^{11}C

*davide.franco@apc.univ-paris7.fr

TABLE I. Scintillator composition used in present and future underground neutrino experiments.

Experiment	Scintillator	Fluor	Dope
KamLAND [4]	20% PC 80% OIL	1.5 g/l PPO	
Borexino [10]	PC	1.5 g/l PPO	
LVD [14]	Paraffin	1.0 g/l PPO	
SNO+ [15]	LAB	PPO	0.1% Nd
Double Chooz [5]	20% PXE 80% OIL	3–6 g/l PPO 20 mg/l Bis-MSB	0.1% Gd
Daya Bay [6]	LAB	3 g/l PPO 15 mg/l Bis-MSB	0.1% Gd
RENO [7]	LAB	1–5 g/l PPO 1–2 mg/l Bis-MSB	0.1% Gd

radioisotopes, which represent a crucial background for the solar neutrino signal in Borexino and KamLAND [12,13].

In this article, we characterize the o-Ps formation probability and lifetime for the most popular choices of scintillator solvents used by present experiments (Table I): 1,2,3-trimetilbenzene or pseudocumene (PC, C_9H_{12}), linear alkyl benzene (LAB, $C_{18}H_{30}$), phenylxylylethane (PXE, $C_{16}H_{18}$), and dodecane (OIL, $C_{12}H_{26}$).

Wavelength shifters are present in scintillators with very low concentrations. However, adding a fluor to scintillators can change the o-Ps properties. For this reason, we studied a typical scintillator mixture, PC + 1.5 g/l of PPO (2,5-diphenyloxazole), to observe the effect of the fluor on the o-Ps properties.

In the second part of the article we discuss the results of Monte Carlo simulations in which we quantify the distortion on the pulse shapes introduced by the o-Ps and the effects on the positron event reconstruction in large volume liquid scintillator detectors.

Finally, we demonstrate that the o-Ps-induced distortion potentially represents a powerful signature for antineutrinos.

II. EXPERIMENTAL APPARATUS

The positron annihilation lifetime spectra have been measured with a fast coincidence system, formed by two plastic scintillators, with a time resolution of 0.28 ns at full width at half maximum (FWHM). ^{22}Na is a β^+ radioisotope, with Q value = 2.842 MeV, emitting positrons in association with 1.274-MeV γ rays (99.94% branching ratio). The ^{22}Na source (0.8 MBq activity) was prepared by drying a droplet of ^{22}Na from a carrier-free neutral solution between two layers, each composed of two Kapton foils (7.5 μm thick, 1-cm radius each single layer). Kapton is a polymide compatible with scintillator materials and where positrons do not form o-Ps states [16,17].

The Kapton-source sandwich is inserted in a glass vial, containing the scintillator sample. The vial is positioned between two plastic scintillator detectors (Pilot U) each of them coupled with a photomultiplier tube. The vial is in direct contact with the faces of the two detectors to maximize the solid angle.

The system measures the delay occurring between the ^{22}Na decay and the positron annihilation: when a plastic scintillator is hit by a 1.274-MeV γ ray, from ^{22}Na decay, the second detector opens a gate of 43 ns in order to detect one of the annihilation γ rays. The time resolution of each detector is $\sim$130 ps.

Discrimination between start and stop events occurs on the basis of the different energies of the detected γ ray. The first detector has a lower threshold at 900 keV to detect the prompt signal from the 1.274-MeV γ ray, while the annihilation γ deposited energy is recorded if it falls in the 350–500 keV energy range. The second energy cut has been optimized to avoid the backscattering of the 1.274-MeV γ rays.

A constant fraction discriminator generates a fast timing signal whenever a γ ray with the correct energy is detected. A time-to-amplitude converter, enabled by the start signal from the discriminator, produces a voltage linearly increasing with time, which stops at the arrival of the stop signal from the other discriminator: the signal at the output of the time-to-amplitude converter is proportional to the time interval elapsed between generation and annihilation of the positron. This signal is finally digitized by an analog-to-digital converter with 4096 channels.

The time interval corresponding to each channel is 10.6 ps, and it is calibrated with a ^{60}Co source. The resolution of the apparatus (0.28 ns at FWHM) is measured by looking at the fast (182 ps) coincidence between the two γ rays emitted by the ^{207}Bi decay, through the $5/2^-$ ^{207}Pb excited state. The detector resolution is modeled with the sum of two Gaussians with different standard deviations.

III. DATA ANALYSIS AND RESULTS

The five samples (PC, PXE, LAB, OIL, PC + PPO) of scintillators have been degassed with nitrogen before each measurement. For each sample, we repeated the measurement, at the ambient temperature, from three to five times, to take into account possible systematics due to changes of the initial conditions (e.g., temperature and time of nitrogen stripping).

The collected total statistics for each sample is $\sim 5 \times 10^6$ events. Measured positron annihilation lifetime distributions of PC and PC + PPO samples are shown in Fig. 1.

Each distribution is fitted with a three-component model:

$$F(t) = \chi(t > t0)\left(\sum_{k=1,2}\frac{A_k}{\tau_k}e^{-t/\tau_k} + C\right), \tag{3}$$

where A_1 and τ_1 correspond to the effective amplitude and mean lifetime of the annihilation and p-Ps components, which cannot be disentangled; A_2 and τ_2 are the o-Ps amplitude and mean lifetime, respectively; C is the flat distribution due to accidental background; t_0 is the detector time offset; and χ is a step function. The fit function $F(t)$ is convoluted with the detector resolution, modeled with the sum of two Gaussians,

$$G(t) = \sum_{i=1,2}\frac{g_i}{\sqrt{2\pi\sigma_i^2}}e^{-\frac{t^2}{2\cdot\sigma_i^2}}, \tag{4}$$

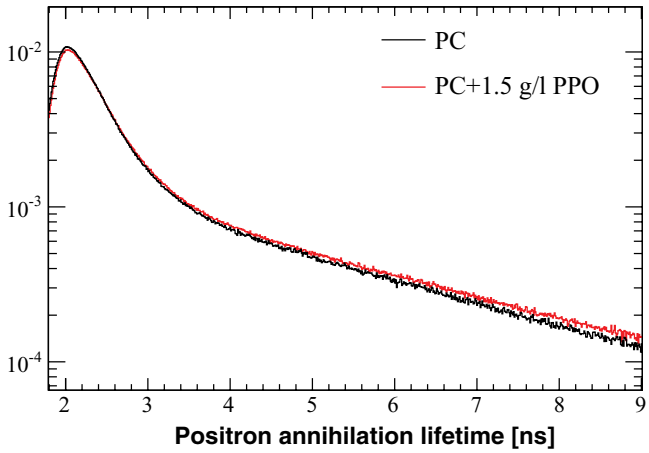

FIG. 1. (Color online) Positron annihilation lifetime spectra for the PC and PC + 1.5 g/l PPO samples.

centered in the same value but with different resolutions (σ_1 and σ_2), and where g_i ($i = 1, 2$) are the relative weights of the two components ($g_1 + g_2 = 1$). The detector resolution is dominated by the Gaussian with $\sigma_1 \sim 110$ ps ($g_1 \sim 0.8$), while $\sigma_2 \sim 160$ ps. The data modeling package used in this analysis is the RooFit toolkit [18], embedded in the ROOT package [19], based on MINUIT. All the parameters in the model are free in the fit. An example of fit for the PXE sample is shown in Fig. 2.

All the normalized χ^2, obtained from the fits, are in the 0.85–0.98 range. Statistical errors for both mean lives and amplitudes are at the order of per mil level. τ_1 is almost constant in all the measurements: the mean τ_1 is centered in 365 ps, with a root mean square of 8 ps.

To estimate the fraction of positrons being annihilated in Kapton, we covered the ^{22}Na source with one to three Kapton layers, identical to those used for characterizing scintillators. The Kapton-source sandwiches were inserted in a Plexiglas medium, characterized by an o-Ps mean lifetime of ∼2 ns. The o-Ps fraction, as a function of the Kapton layers, is fitted with an exponential, as shown in Fig. 3. We estimate that

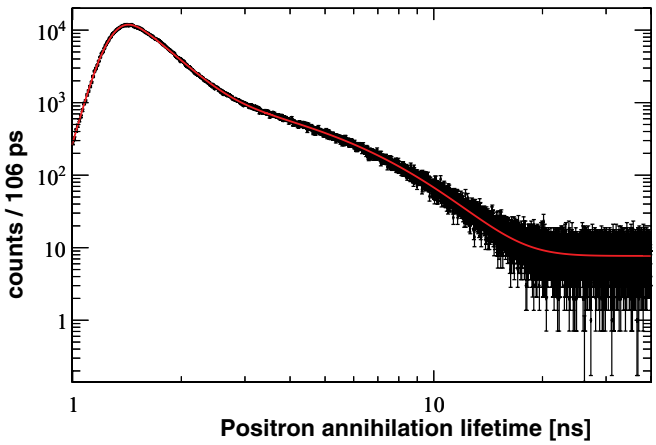

FIG. 2. (Color online) Fit (red line) of the positron annihilation lifetime spectrum (black dots) for the PXE sample.

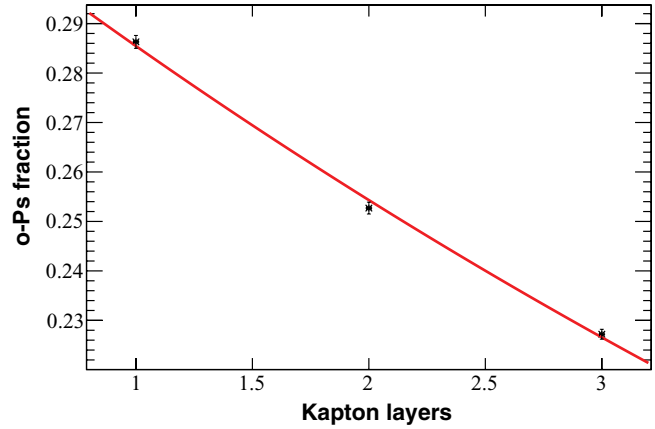

FIG. 3. (Color online) The data points represent the o-Ps fraction, measured with one to three Kapton layers, inserted in a Plexiglas medium. Each layer is 7.5 μm thick and 1 cm in radius. The line is the result of an exponential fit.

20.6% ± 0.2% of positrons are annihilated in the double Kapton layer (15 μm thick).

In order to derive the o-Ps formation probability (f_2) in the analyzed liquid scintillator samples, we subtract the annihilation component in Kapton (A_K):

$$f_2 = \frac{A_2}{A_1 + A_2 - A_K}. \tag{5}$$

To estimate the systematic uncertainties, we evaluated first the o-Ps mean lifetime weighted averages of all the measurements for each sample. We fitted then the distribution of all the deviations of each measurement from the correspondent weighted average with a Gaussian, in a likelihood approach. The same procedure was applied also for the o-Ps formation probability. The resulting systematic errors for the o-Ps fraction and mean lifetime are 0.5% and 0.03 ns, respectively, and dominate over the statistical errors. The final results are shown in Table II and in Fig. 4.

All the samples analyzed in this paper are characterized by an o-Ps mean lifetime of about 3 ns and a formation probability of about 50%. The o-Ps mean lifetime and fraction for PXE and LAB represent the extremes in the value ranges: PXE (LAB) is the solvent where o-Ps has the lowest (largest) probability to be formed and the shortest (longest) lifetime.

Kino *et al.* [20] characterized the o-Ps properties on a PC sample saturated with N_2 with a similar experimental setup. The resulting mean lifetime (3.03 ± 0.02 ns) is compatible within 2 σ with the one reported in this article, while

TABLE II. Final results for the o-Ps probability formation and mean lifetime for the analyzed samples of scintillators.

Material	f_2	τ_2 (ns)
PXE	0.466 ± 0.005	2.74 ± 0.03
LAB	0.542 ± 0.005	3.08 ± 0.03
PC	0.485 ± 0.005	2.96 ± 0.03
OIL	0.506 ± 0.005	3.04 ± 0.03
PC+1.5 g/l PPO	0.512 ± 0.005	3.12 ± 0.03

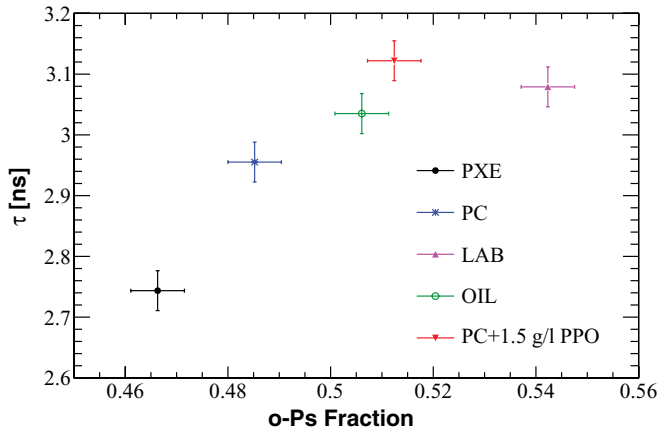

FIG. 4. (Color online) Results of the o-Ps probability formation and mean lifetime for the analyzed samples of scintillators.

we observe a formation probability 5.2% larger. This small discrepancy can be attributed to a not identical concentration of oxygen [20] in the scintillator sample or to different condition parameters, like temperature (the o-Ps formation probability as a function of the temperature has been discussed by Zgardzinska *et al.* [21]), during the measurements.

IV. o-Ps-INDUCED PULSE SHAPE DISTORTION

Positrons and the following annihilation γ rays , even after o-Ps formation, cannot be disentangled in large volume liquid scintillator detectors, like Double Chooz, Borexino, and KamLAND, by looking at the photon arrival times in the photomultiplier tubes. Such experiments are, in fact, characterized by time constants, like the fluorescence decay time (Table III) and the photomultiplier tube time jitters, typically longer than the delay between positrons and annihilation γ-ray emission.

However, the o-Ps formation can induce a significant distortion in the pulse shape of positrons. In positron detection, scintillator molecules are first excited by positron interactions and then by annihilation γ rays. If annihilation passes through the intermediate o-Ps state, the annihilation component is delayed, and the overall photon emission time distribution (PETD) results as the sum of the two components, as shown in Fig. 5 for 0.5-MeV positrons in PC + 1.5 g/l PPO, annihilating after o-Ps formation. The correspondent PETD deformation, with respect to the direct positron annihilation case, is dominant in the first 30 ns.

TABLE III. Scintillator decay time constants (τ_i) and amplitudes (N_i) for β particles for PC + 1.5g/l PPO [22], PXE + 1.0 g/l PPO [23], and LAB + 1.0 g/l PPO [23].

Scintillator	τ_1 (ns)	τ_2 (ns)	τ_3 (ns)	N_1 %	N_2 %	N_3 %
PC + 1.5 g/l PPO	3.57	17.61	59.9	89.5	6.3	4.2
PXE + 1.0 g/l PPO	3.16	7.7	34	84.0	12.0	2.9
LAB + 1.0 g/l PPO	7.46	22.3	115	75.9	21.0	3.1

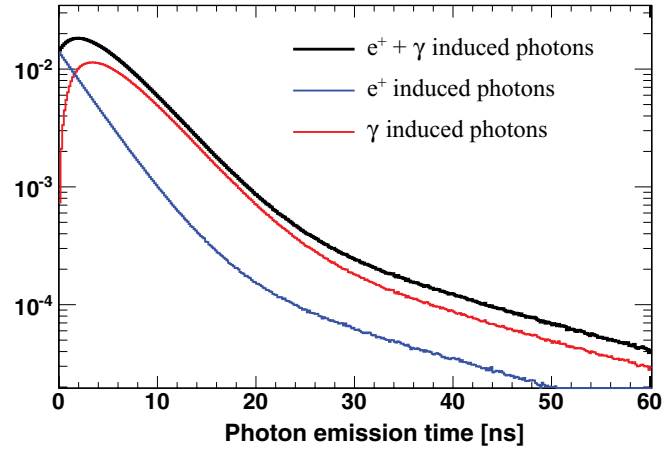

FIG. 5. (Color online) Simulation of the photon emission time (black/top line) induced by 0.5-MeV positrons, all forming o-Ps, in the PC + 1.5 g/l PPO scintillator. The scintillation components, due to positrons (blue/bottom line) and o-Ps decay γ rays (red/middle line), are shown separately.

The distortion is energy dependent, since the amplitude of the first component is proportional to the positron energy, while the γ component has fixed energy. To study such dependency, we simulated positrons with energies from 0.1 to 5.0 MeV. The ratio (R) of the PETD mean values between the o-Ps and the direct annihilation cases is plotted in Fig. 6. It is notable that the deformation of the time distribution is larger for lower energy positrons, where R can reach up to ∼1.6. At higher energies, the distortion reaches a plateau, with o-Ps PETD mean values shifted up to 10%, depending on the scintillator composition.

In neutrino experiments, the o-Ps-induced PETD deformation can have an impact on several algorithms for the event reconstruction and discrimination. For instance, the position reconstruction algorithms (e.g., Smirnov [24]) strongly depend on the first ($t < 30$ ns) detected photoelectrons. A bias

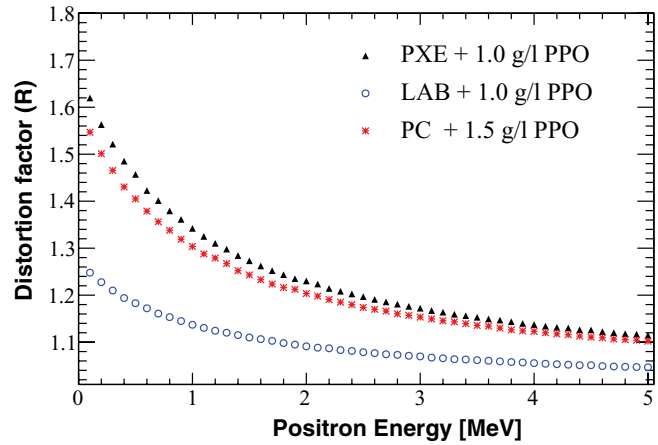

FIG. 6. (Color online) Ratio between the mean values of the o-Ps and direct annihilation photon emission time distributions as function of the positron energy for PXE + 1.0 g/l PPO, LAB + 1.0 g/l PPO, and PC + 1.5 g/l PPO, assuming the scintillation decay constants from Table III.

in the position reconstruction can induce a further bias in the event energy reconstruction, because the light collection on the photomultiplier tubes depends on the reconstructed position. Also algorithms for particle discrimination in liquid scintillators can be strongly affected, because they rely on the dependence of fast and slow portions of the scintillation pulse on the energy loss of the interacting particle [22,25].

V. POSITRONIUM SIGNATURE

Beyond the necessity to minimize systematics in the event reconstruction, the o-Ps-induced pulse shape distortion potentially provides a signature for tagging positrons and hence for enhancing the neutrino detection. Borexino and KamLAND could directly benefit by a positron/electron discrimination by enhancing the tagging and rejection of cosmogenic ^{11}C β^+ decay, the main background component in the *pep* and Carbon-Nitrogen-Oxygen Cycle (CNO) solar neutrino energy window [12,13]. Also θ_{13} and geoneutrino experiments could be advantaged by discriminating cosmogenic ^{9}Li and ^{8}He β-neutron decays that mimic the antineutrino signal.

To quantify the o-Ps and the direct annihilation positron event discrimination, we simulate an ideal spherical detector (4 m in radius), with 2000 photomultiplier tubes. The simulation is GEANT4 based. The cathode is a segment of a 20-cm-radius sphere. The scintillator is PC + 1.5 g/l PPO, and its properties are taken from Elisei *et al.* [26]. The scintillation photon yield is 10 000 photons/MeV. The simulation includes optical effects, like Rayleigh scattering, absorption and reemission, and reflections on cathodes and on the spherical steel structure.

We simulated samples of 10 000 positron events, in the detector center, directly annihilated or annihilated following the o-Ps formation. Positrons, directly annihilated, have the identical pulse shapes of equivalent electrons with the same energies plus 1.022 MeV, from annihilation γ rays. Positrons, in fact, thermalize in 300 ps, much faster than the characteristic scintillation decay times, and γ rays release energy mainly through Compton electron cascades. In the simulation, positron energy varies from 0.1 to 5 MeV. To take into account the photomultiplier tube jitter, we smeared the photoelectron time distribution by 1.4 ns and we assume an ideal fast electronic chain based on 1-GHz Flash-ADC. The photoelectron time distributions (Fig. 7) are relative to the first detected photoelectron.

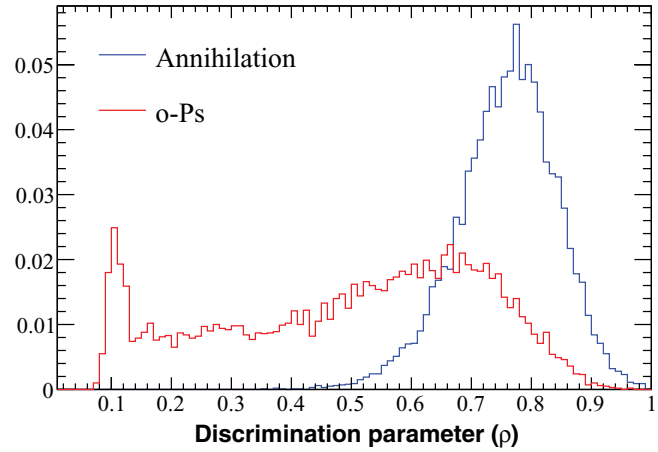

FIG. 8. (Color online) ρ distributions for 0.5-MeV positrons directly being annihilated (blue line/line with highest peak) and forming o-Ps (red line/line with lowest peak). Both the distributions are normalized to one event.

The pulse shapes differ particularly in the peak positions and widths. We define a discrimination variable, ρ, as the ratio between the integrals of the distributions between 0–18 ns and 18–60 ns. An example of ρ distribution for 0.5-MeV positrons is shown in Fig. 8. Even with a not sophisticated estimator, the separation between the two samples is clear: ρ from direct annihilation positrons is Gaussian distributed, centered in 0.76, while positrons following the o-Ps decay

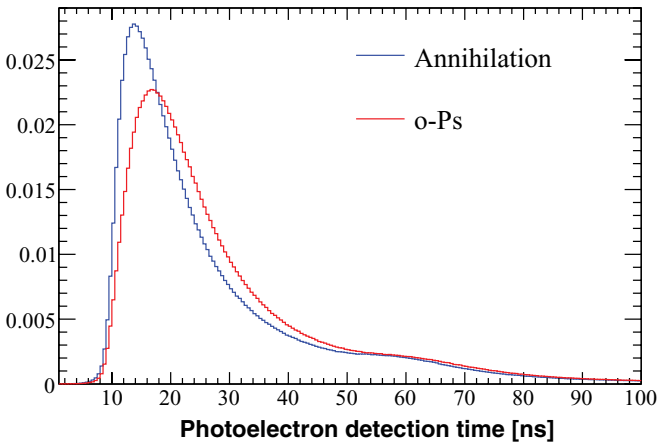

FIG. 7. (Color online) Photoelectron time distributions from an ideal 4-m-radius detector, filled with PC + 1.5 g/l PPO, for 0.5-MeV positrons being directly annihilated (blue line/line with highest peak) and forming o-Ps (red line/line with lowest peak). The structure at ∼60 ns is due to optical reflections on detector materials. Both the distributions are normalized to one event.

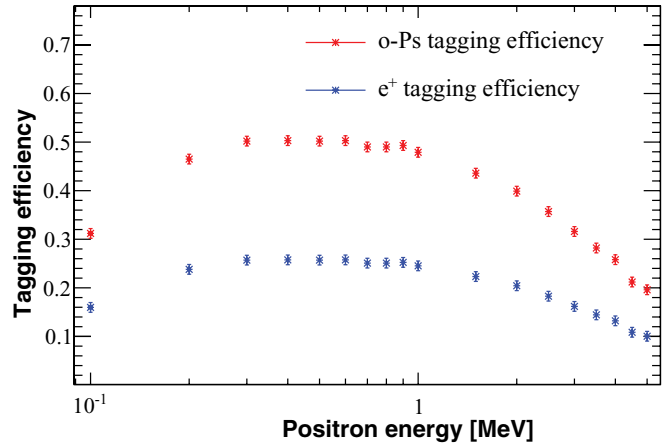

FIG. 9. (Color online) o-Ps tagging efficiency (red/top points) based on the $\rho < \rho_0(E)$ cut, requiring 1% of direct annihilation contamination fraction, for an ideal 4-m-radius detector filled with PC + 1.5 g/l PPO. The e^+ tagging efficiency (blue/bottom points) is obtained by multiplying the o-Ps tagging efficiency by the o-Ps formation probability.

have a broad distribution of ρ, depending on the o-Ps lifetime. Because of the already mentioned energy dependence, we optimized the $\rho < \rho_0(E)$ cut by varying the $\rho_0(E)$ threshold with the requirement of 1% direct annihilation contamination fraction. The results are shown in Fig. 9. The lower efficiency detection at 100 keV, with respect to the one at 500 keV, is due to the detector resolution.

With this technique, we demonstrate that an event by event tagging of positrons is possible, with efficiency as high as ∼25% at 0.5 MeV, equal to the detection efficiency multiplied by the o-Ps formation probability. More sophisticated algorithms can improve the positronium detection efficiency, providing a new signature for antineutrino experiments and for background rejections in solar neutrino experiments

VI. CONCLUSIONS

In this article we measured the o-Ps formation probabilities and lifetimes for the most popular organic liquid scintillators used in neutrino experiments. All the scintillators are characterized by similar o-Ps properties, with ∼3 ns mean lifetime and ∼50% formation probability. The distortion of PETD induced by the o-Ps intermediate state is a source of systematic in neutrino experiments, because it affects positron event reconstruction and pulse shape discrimination algorithms.

We further demonstrated that the o-Ps-induced distortion represents a powerful signature for discriminating a fraction of positrons from electrons. This technique can be exploited both for enhancing the antineutrino detection efficiency in θ_{13} and geoneutrino experiments and for rejecting the positron background in solar neutrino experiments.

ACKNOWLEDGMENTS

We are grateful to Ute Schwan, Stefan Schoenert, and Paolo Lombardi for providing us with the scintillator samples. We thank also Simone Stracka, Pietro Biassoni, and José Maneira for useful discussions and comments.

[1] G. Bellini *et al.*, Phys. Lett. B **687**, 299 (2010).
[2] T. Araki *et al.*, Nature (London) **436**, 499 (2005).
[3] G. L. Fogli, E. Lisi, A. Palazzo, A. M. Rotunno, Phys. Rev. D **82**, 093006 (2010).
[4] K. Eguchi *et al.*, Phys. Rev. Lett. **90**, 021802 (2003).
[5] F. Ardellier *et al.*, arXiv:hep-ex/0606025.
[6] Xin-Heng Guo *et al.*, arXiv:hep-ex/0701029.
[7] K. K. Joo *et al.*, Nucl. Phys. Proc. Suppl. **168**, 125 (2007).
[8] A. Bernstein *et al.*, J. Appl. Phys. **91**, 4672 (2002).
[9] M. Deutsch, Phys. Rev. **82**, 455 (1951).
[10] G. Alimonti *et al.*, Nucl. Instrum. Methods Phys. Res. Sect. A **600**, 568 (2009).
[11] S. Abe *et al.*, Phys. Rev. Lett. **100**, 221803 (2008).
[12] M. Balata *et al.*, Phys. Rev. C **74**, 045805 (2006).
[13] C. Galbiati, A. Pocar, D. Franco, A. Ianni, L. Cadonati, and S. Schonert, Phys. Rev. C **71**, 055805 (2005).
[14] G. Bari *et al.*, Nucl. Instrum. Methods Phys. Res. Sect. A **277**, 11 (1989).
[15] M. C. Chen., arXiv:0810.3694.
[16] S. McGuire and D. J. Keeble, J. Phys. D Appl. Phys. **39**, 3388 (2006).
[17] K. Plotlowski, T. J. Panek, and J. Kansy, Nuovo Cimento D **10**, 933 (1988).
[18] W. Verkerke *et al.*, arXiv:physics/0306116.
[19] R. Brun and F. Rademakers, Nucl. Instrum. Methods Phys. Res. Sect. A **389**, 81 (1997).
[20] Y. Kino *et al.*, J. Nucl. Radiochem. Sci. **1**, 63 (2000).
[21] B. Zgardzinska *et al.*, Acta Phys. Pol. A, **110**, 747 (2006).
[22] H. O. Back *et al.*, Nucl. Instrum. Methods Phys Res. Sect. A **584**, 98 (2008).
[23] T. Marrodan Undagoitia *et al.*, Rev. Sci. Instrum. **80**, 043301 (2009).
[24] O. Ju. Smirnov, Instrum. Exp. Tech. **46**, 327 (2003).
[25] E. Gatti and F. DeMartini, Nucl. Electron. IAEA Vienna **2**, 265 (1962).
[26] F. Elisei *et al.*, Nucl. Instrum. Methods Phys Res. Sect. A **400**, 53 (1997).